ACS APPLIED BIO MATERIALS

Cite This: ACS Appl. Bio Mater. 2018, 1, 1793−1799

Letter

www.acsabm.org

Laser-Activated Self-Assembled Thermoplasmonic Nanocavity Substrates for Intracellular Delivery

Marinna Madrid,[*,⊥,†] Nabiha Saklayen,[⊥,‡] Weilu Shen,[†] Marinus Huber,[§] Nicolas Vogel,[∥] and Eric Mazur[†,‡]

[†]Department of Applied Physics, School of Engineering and Applied Sciences and [‡]Department of Physics, Harvard University, Cambridge, Massachusetts 02138, United States

[§]Department of Physics, Ludwig Maximilian University of Munich, Munich, 80539, Germany

[∥]Institute of Particle Technology, Friedrich-Alexander University Erlangen-Nürnberg, Erlangen, 91058, Germany

Supporting Information

ABSTRACT: Intracellular delivery is crucial for cellular engineering and the development of therapeutics. Laser-activated thermoplasmonic nanostructured surfaces are a promising platform for high-efficiency, high-viability, high-throughput intracellular delivery. Their fabrication, however, typically involves complicated nanofabrication techniques, limiting the approach's applicability. Here, colloidal self-assembly and templating are used to fabricate large arrays of thermoplasmonic nanocavities simply and cost-effectively. These laser-activated substrates are used to deliver membrane-impermeable dye into cells at an efficiency of 78% and throughput of 30 000 cells min^{-1} while maintaining 87% cell viability. Proof-of-concept data show delivery of large cargoes ranging from 0.6 to 2000 kDa to cells without compromising viability.

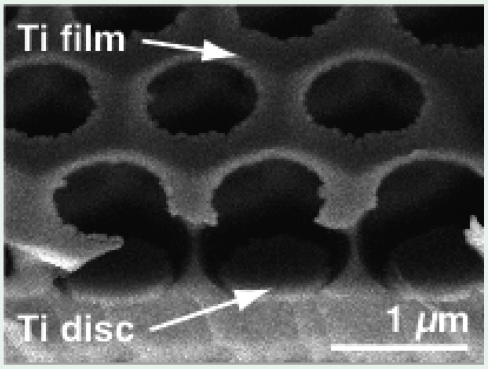

KEYWORDS: *intracellular delivery, self-assembly, colloidal templating, thermoplasmonics, pulsed lasers*

The delivery of membrane-impermeable cargoes such as nanoparticles, genetic materials, or functional proteins directly into cells is a critical step for applications in medical research, such as the manipulation of cells and tissues for regenerative medicine or the engineering of cells for personalized cell therapies.[1] Intracellular delivery methods include biological vectors, such as viruses, chemical modifications of delivery cargoes, such as lipofection, and physical techniques, such as microinjection, electroporation, and optoporation.[2,3] While research efforts have led to a continuous increase in efficiency and sophistication, each of the approaches faces inherent limitations.

For instance, viral-based delivery offers high-efficiency delivery at high throughput but is limited in terms of cargo-carrying capacity, the ability to only deliver genetic material, and the potential for immunologic and oncogenic risks.[2] Lipofection is a high-throughput chemical technique, but it is cell-type specific, can require complex customization for different cargo types, and suffers from endosomal trapping of cargoes.[2] Electroporation, a widely used physical delivery method that offers both high delivery efficiency and high throughput for a range of cargo types, often results in low cell viability , particularly for sensitive cell types.[2] Other physical techniques, such as microinjection, sonoporation, magnetofection, and microfluidic squeezing, are ideal for certain applications but are limited in terms of applicability to sensitive, difficult-to-transfect cell types.[2] To this point, no platform technology exists that combines highly efficient delivery while maintaining cell viability, with high throughput processing, versatility with respect to type of cell and cargo, and simple, cheap, and affordable production.

Optoporation, a physical delivery technique, utilizes a tightly focused laser beam to create a transient pore in the cell membrane.[3] This technique offers high delivery efficiency and high cell viability. As a consequence of the physical nature of the process, optoporation is inherently versatile with respect to the chemical nature of the cargo and the cell type to be used. However, each cell must be porated individually by focusing the laser beam directly onto the membrane, putting limitations on the throughput. Modifications, including the use of active flow in microfluidic channels and a nondiffracting beam, slightly increase the throughput but not to the scale necessary for therapeutic applications, which require on the order of 1×10^8 cells.[3] Laser-activated thermoplasmonic nanostructures improve the throughput of this delivery technique by efficiently absorbing the laser energy at multiple localized hotspots and transferring energy to the surrounding medium.[4] This transfer of energy to the surrounding solution results in the creation of a bubble or pressure wave that generates a transient pore in the cell membrane.[5−7] Gold nanoparticles have been used to

Received: September 11, 2018
Accepted: October 25, 2018
Published: October 25, 2018

DOI: 10.1021/acsabm.8b00447
ACS Appl. Bio Mater. 2018, 1, 1793−1799

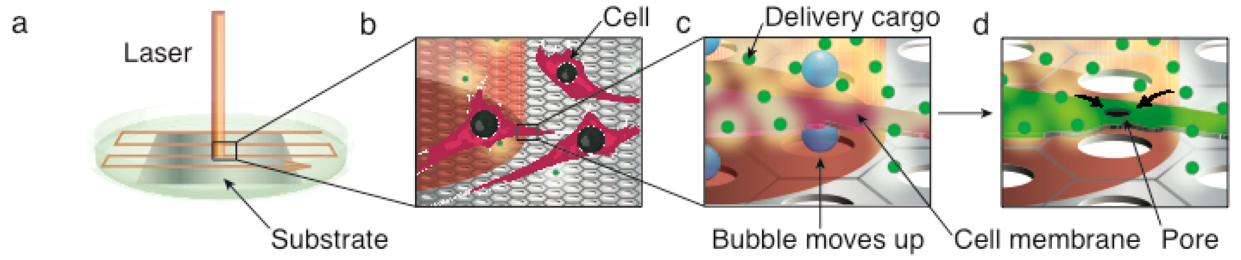

Figure 1. Schematic illustration of intracellular delivery using a self-assembled laser-activated thermoplasmonic nanocavity substrate. (a) A thermoplasmonic nanocavity substrate is placed at the bottom of a Petri dish. HeLa CCL-2 cells are cultured onto the substrate, and the laser beam is scanned across the sample. (b) The laser beam spot illuminates specific regions of the self-assembled thermoplasmonic substrate, enabling spatially selective intracellular delivery to the cells cultured in those regions. (c) The laser light energy is absorbed by the metallic nanostructures, resulting in localized heating and the formation of bubbles in the surrounding cell medium. (d) The bubbles form transient pores in the cell membrane, permitting membrane-impermeable target molecules in the surrounding cell medium to diffuse into the cell through the pores. After the pores heal, the target molecules are enclosed in the cell, concluding the light-activated intracellular delivery.

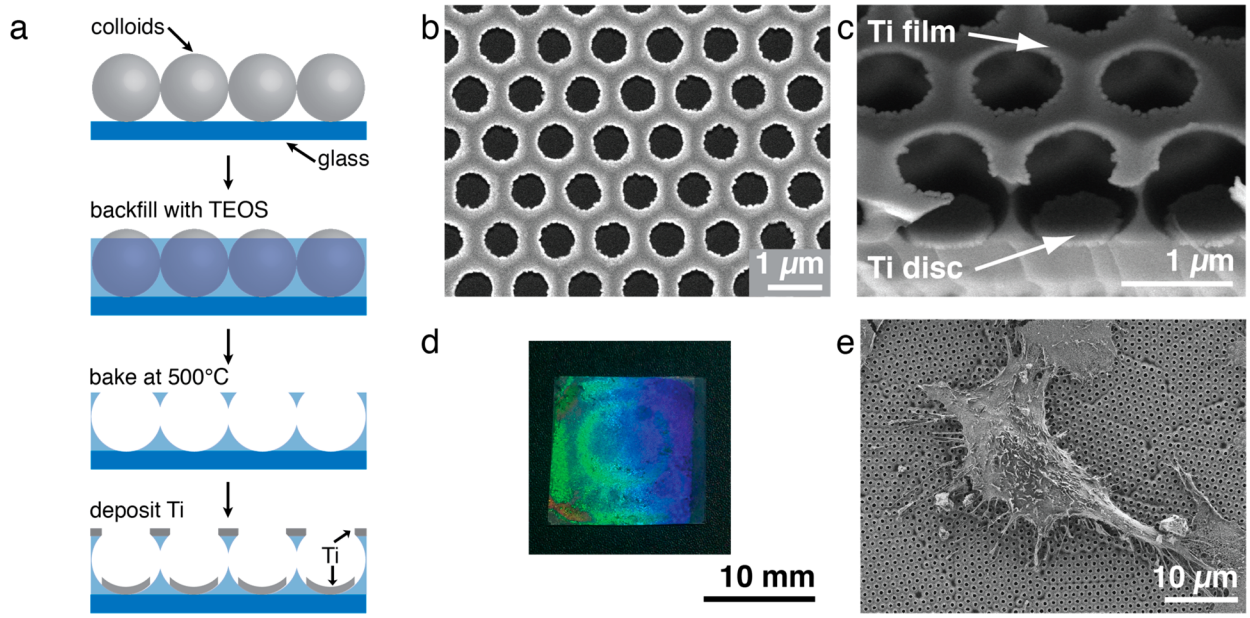

Figure 2. Fabrication and characterization of self-assembled thermoplasmonic nanocavity substrates. (a) Fabrication process for the thermoplasmonic nanocavity substrate. A close-packed monolayer of monodispersed polystyrene colloidal particles is deposited onto a glass substrate. Subsequently, the monolayer is backfilled with tetraethylorthosilicate (TEOS), a liquid glass precursor material. Calcination at 500 °C combusts the organic colloid material, leaving an array of nanopores at the surface. A thin layer of titanium is finally deposited by directed evaporation, producing a continuous film at the pore surfaces and individual discs at the bottom of the pores. (b) Top-view SEM image of nanocavities. The cavities are ∼1 μm in diameter with pore openings of ∼800 nm. (c) Tilted SEM image of nanocavities, showing the continuous porous Ti film on top of the nanocavities and the disconnected Ti discs at the bottom. (d) Photographic image of a thermoplasmonic nanocavity substrate. (e) SEM image of chemically fixed HeLa CCL2 cell on the nanocavities. Each cell covers ∼300 to 700 nanocavities, depending on the size of the cell.

porate cell membranes with high efficiency, high viability, and high throughput for a range of cell types.[8] However, the gold nanoparticles remain in the cell after delivery as metallic residue and can form aggregates, which may cause toxicity in the long term.[9] Laser-activated nanostructured substrates bypass this limitation, as cells can be cultured on the substrates, porated, and removed from the substrates (which remain intact) after intracellular delivery without leaving metallic particles within the cells.[10−13]

While laser-activated nanostructured substrates are a promising option for intracellular delivery, their small feature sizes typically require nanofabrication techniques that are serial in nature, and necessitate expensive and sophisticated instrumentation and clean room infrastructure.[10−13] These limitations hinder a widespread use of these substrates in research and technology.

An alternative to nanofabrication is the design of nanostructures from the bottom-up through self-assembly processes to direct suitable building blocks into ordered arrangements of periodic surface structures over macroscopic areas. Colloidal self-assembly employs spherical colloidal particles—which can be conveniently synthesized at nanoscale dimensions using scalable synthesis protocols—as building blocks to create well-ordered arrangements in two and three dimensions.[14,15] These colloidal crystals can serve as templates to create nanoporous materials: A second material, typically sol−gel derived silica, is deposited within the interstitial sites of the polymer colloidal crystal to create a porous layer after removal of the templating colloidal particles.[16,17] Note that,

DOI: 10.1021/acsabm.8b00447
ACS Appl. Bio Mater. 2018, 1, 1793−1799

while the term nanopores in some communities is exclusively used for pore dimensions much below 100 nm, porous materials prepared by colloidal templating are also typically referred to as nanopores,[16,17] even though the dimensions are typically in the range of 100−1000 nm. Alternatively, a directed metal deposition step can produce defined metal nanostructure arrays by exploiting the shadowing effect of the colloidal particles on the surface.[18,19] Colloidal self-assembly therefore provides a platform to create defined, functional nanostructure arrays in a simple, fast, and scalable fashion.[15,16,20]

Here, we employ colloidal self-assembly and templating to design defined thermoplasmonic nanocavity arrays over macroscopic areas. We show that these structures permit efficient laser-activated cell poration with high throughput and high spatial resolution, enabling the delivery of model components with different molecular weights with high efficiency and cell viability.

Figure 1 shows the delivery of membrane-impermeable cargoes into cells using a laser-activated self-assembled thermoplasmonic nanocavity substrate. The substrate consists of silica nanocavity structures coated with a thin titanium (Ti) film. Upon illumination with a nanosecond pulsed laser, the laser energy is absorbed by the metallic nanostructures and converted into thermal energy, resulting in localized heating.[4,21] This high and rapid heating results in the formation of bubbles in the surrounding aqueous environment.[5−7,13,22,23] When cells are cultured on the substrate, these bubbles porate the cell membrane that is in contact with the substrate. Membrane-impermeable molecules in the surrounding cell medium then diffuse through these pores into the cell before the cell membrane heals and seal the pores, encapsulating the cargo within the cell.

We use colloidal self-assembly and templating for the fabrication of the substrates, as schematically illustrated in Figure 2a. In the process, we take advantage of the ability of monodisperse colloidal particles to form close-packed, two-dimensional crystals at the air/water interface. These close-packed, two-dimensional assemblies form as a result of attractive capillary forces acting on the colloidal particles at the air/water interface.[18] We follow a protocol from literature and transfer a preassembled monolayer of polystyrene colloidal particles to a glass coverslip.[24] The colloidal monolayer is then backfilled with tetraethylorthosilicate as the silica sol−gel precursor material. The concentration of the sol−gel precursor is chosen to partially fill the colloidal monolayer, embedding the polymer colloids in a silica matrix.[25] Upon calcination at 500 °C, the organic colloidal particles combust, resulting in an array of nanocavities, termed an inverse colloidal monolayer.[25,26] Finally, 50 nm of Ti is thermally evaporated onto these nanocavities to form the thermoplasmonic substrate. A detailed description of the fabrication process is in the Supporting Information (Section 1). We chose titanium over gold, which is commonly chosen for thermoplasmonic intracellular delivery applications, because our simulation results show Ti-coated nanocavities absorb laser energy more strongly at the operating wavelength of 1064 nm than Au-coated nanocavities (Supporting Information, Section 2, Figure S1). The directed Ti deposition results in two distinct titanium surface structures: a continuous porous Ti film on top of the nanocavities and a Ti disc at the bottom of each nanocavity. The thin metal film and nanostructures enable these substrates to efficiently absorb laser light energy and convert it to thermal energy, resulting in highly localized heating both around the Ti discs and the porous Ti film, thereby providing ideal thermoplasmonic properties for intracellular delivery by optoporation.[22] A top-view scanning electron microscopy (SEM) of the thermoplasmonic nanocavity substrate shows the uniform and regular arrangement of the nanopore array with pore diameters ranging in diameter from ∼750 to 850 nm. The hexagonal symmetry of the pores reflects the symmetry of the colloidal templates (Figure 2b). The diameter of the pores is determined by the concentration of the sol−gel solution and can be precisely adjusted. The presence of the titanium nanostructures as a continuous film with nanopores and separated, individual discs at the bottom of the nanopores can be directly seen in the inside-view SEM images (Figure 2c). The diameter of the cavities is ∼1 μm and is determined by the size of the colloids used to form the monolayer.

Figure 2d shows a photograph of a thermoplasmonic nanocavity substrate completely and homogeneously covering a 14 mm by 14 mm glass coverslip. The structural coloration arising from the nanostructured surface coating demonstrates the high degree of uniformity of the self-assembled thermoplasmonic substrate over macroscopic dimensions.

Figure 2e shows the morphology of a chemically fixed HeLa CCL-2 cell on one of the nanocavity substrates (see Supporting Information, Section 3 for details of the cell fixing process). Each HeLa CCL-2 cell covers several hundred nanocavities, with the exact number of nanocavities determined by the size of the cell and how it adheres to the region. The density of nanocavities can be modified by altering the size of the templating colloidal particles, enabling the optimization of the number of nanocavities per cell and thus the poration efficiency for any chosen cell type.

We investigate the thermoplasmonic poration-induced delivery of molecules into HeLa CCL-2 cells as a function of laser intensity. As a model delivery molecule, we chose calcein green, a 0.623 kDa-sized membrane-impermeable green fluorescent dye. We use fluorescence microscopy to quantify the efficiency of delivery and viability of the cells as a function of the fluence of the applied laser pulses (see Supporting Information, Section 4 for a description of the fluorescence microscopy and cell counting procedure). HeLa CCL-2 cells are cultured on the nanocavity substrate before being scanned with a nanosecond-pulsed laser (see Supporting Information, Section 5 for a description of the cell culture and seeding methods; see Supporting Information, Section 6 for details of the laser scanning setup and technique). Only the cells in the laser-scanned region are porated, enabling the diffusion of membrane-impermeable calcein green dye into cells in the irradiated area. Cells expressing green fluorescence indicate successful intracellular delivery of the molecule. As shown in Figure 3a, only substrate regions that have been exposed to laser light produce cells with green fluorescence, while unexposed surfaces remain dark, demonstrating the absence of dye uptake without light irradiation. Importantly, this thermoplasmonic delivery technique provides a high spatial selectivity of the delivered molecules, which may open pathways for the delivery of required substances to defined regions of an engineered tissue. Figure 3b shows a fluorescence microscopy image of HeLa CCL-2 cells on nanocavity substrates that were porated to take up membrane-impermeable calcein green dye. We tested the cell viability by staining the cells with calcein red-orange AM 4 h after laser-scanning the substrate. Figure 3c shows that the porated and transfected

DOI: 10.1021/acsabm.8b00447
ACS Appl. Bio Mater. 2018, 1, 1793−1799

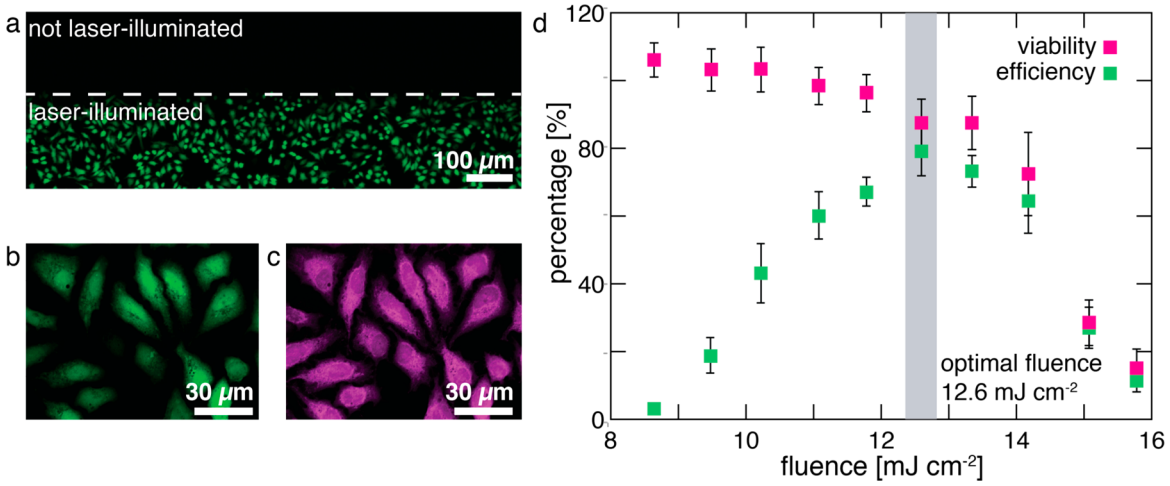

Figure 3. Efficient and spatially-selective intracellular delivery using self-assembled thermoplasmonic nanocavity substrates. (a) Cells are porated and take up fluorescent dye, only in the region irradiated by the laser, demonstrating spatially selective poration. (b) HeLa CCL-2 cells fluoresce green upon poration and uptake of membrane-impermeable calcein green dye. (c) The same cells fluoresce after incubation with viability indicator calcein AM, indicating that these cells exhibit healthy metabolic activity and remain viable after laser treatment. (d) The nanocavity substrates are laser scanned over a range of laser fluences to determine the optimal fluence for maximizing delivery efficiency while maintaining cell viability. Cell counting of fluorescence images indicates a delivery efficiency of ∼78% and a viability of 87% at a laser fluence of ∼12.6 mJ/cm^2. Data represent mean ± standard error from n = 5 data sets.

cells also express a calcein red-orange AM signal, indicating viability.

To maximize delivery efficiency and cell viability we scanned a single thermoplasmonic nanocavity substrate varying the laser fluence in different locations, repeating the experiment five times (Figure 3d). The laser beam was scanned across the substrate by moving the stage holding the sample at a speed of 10 mm s^{-1}, which equates to a throughput of ∼30 000 cells min^{-1}. This throughput could be easily scaled up by, for example, using galvo-scanning mirrors to scan the laser beam across the sample.[27] To quantify the delivery efficiency and cell viability, we imaged the cells after exposure to the laser light using fluorescence microscopy and performed automated cell counting on the images. The delivery efficiency is defined as the number of cells that contain calcein green dye within a laser-irradiated region divided by the total number of cells in a nonlaser-irradiated region of the same size. The viability is defined as the number of cells that express a calcein AM signal within a laser-irradiated region, divided by the total number of cells in a nonlaser-irradiated region of the same size. It is important to note that, because the cell density is not perfectly uniform across a single substrate, viability values above 100% can result from the normalization procedure. At a laser fluence of 8.7 mJ cm^{-2}, we observe a delivery efficiency of 4% and a cell viability of 105%. As the laser fluence is increased to 12.6 mJ cm^{-2}, the delivery efficiency increases, while the cell viability remains above 85%. At a laser fluence of 12.6 mJ cm^{-2}, we observe a delivery efficiency of 78% and a cell viability of 87%. This delivery efficiency is 4.3 times higher than the delivery efficiency observed for a comparison experiment, where a 50 nm thin film of Ti was evaporated directly onto an unstructured glass coverslip before being seeded with cells and scanned with a pulsed laser. In the case of the Ti-coated glass coverslip, we observe an 18% delivery efficiency and 88% viability at an optimum laser fluence of 10.8 mJ cm^{-2} (Supporting Information, Section 7, Figure S3). It is worth noting that, although the glass coverslip is unstructured, the evaporated Ti does have some surface roughness that likely mediates bubble formation upon laser irradiation (Supporting Information, Section 8, Figure S4). As the laser fluence increases above 12.6 mJ cm^{-2}, the cell viability and delivery efficiency both decrease. The delivery efficiency decreases along with cell viability because calcein green only remains inside cells that are viable and have an intact cell membrane. At a laser fluence of 15.8 mJ cm^{-2}, we observe a delivery efficiency of 12% and a cell viability of 16%. These results show that we obtain maximum delivery efficiency at a fluence of 12.6 mJ cm^{-2}.

In previous work, we used nanofabricated pyramids with 2.4 μm baselengths and edge-to-edge spacings of 1.2 μm covered in a 50 nm thin layer of gold (Au) to deliver calcein green dye to HeLa CCL-2 cells.[13] For the thermoplasmonic micropyramid substrates, we determined the optimal fluence to be 54 mJ cm^{-2}, which is ∼5 times higher than the 12.6 mJ cm^{-2} optimal fluence observed for the nanocavity substrates. The maximum calcein green delivery efficiency of 78% for the nanocavity substrates is slightly less than the 95% delivery efficiency measured for the micropyramid substrates. However, unlike with the micropyramid substrates, the fabrication process for the nanocavity substrates does not require the use of sophisticated and expensive cleanroom equipment. The same nanosecond-pulsed laser system and scanning parameters were used for both sets of experiments. The lower optimal fluence for the nanocavity substrates may indicate that the Ti-coated nanocavities are more efficient at absorbing and converting laser energy than the Au-coated micropyramids or may be due to the higher density of nanocavities on the patterned substrates compared to the micropyramids.

Many membrane-impermeable cargoes of interest in biomedical research are orders of magnitude larger than the calcein green dye (0.6 kDa) used for our fundamental investigations. For instance, siRNA, a key component in gene therapy, has a molecular weight of ∼13 kDa.[28] Proteins such as the CRISPR-Cas9 ribonucleoprotein complex, a powerful gene-editing tool, and antibodies, which are of interest for imaging, are ∼150 kDa.[1] To investigate the

DOI: 10.1021/acsabm.8b00447
ACS Appl. Bio Mater. 2018, 1, 1793−1799

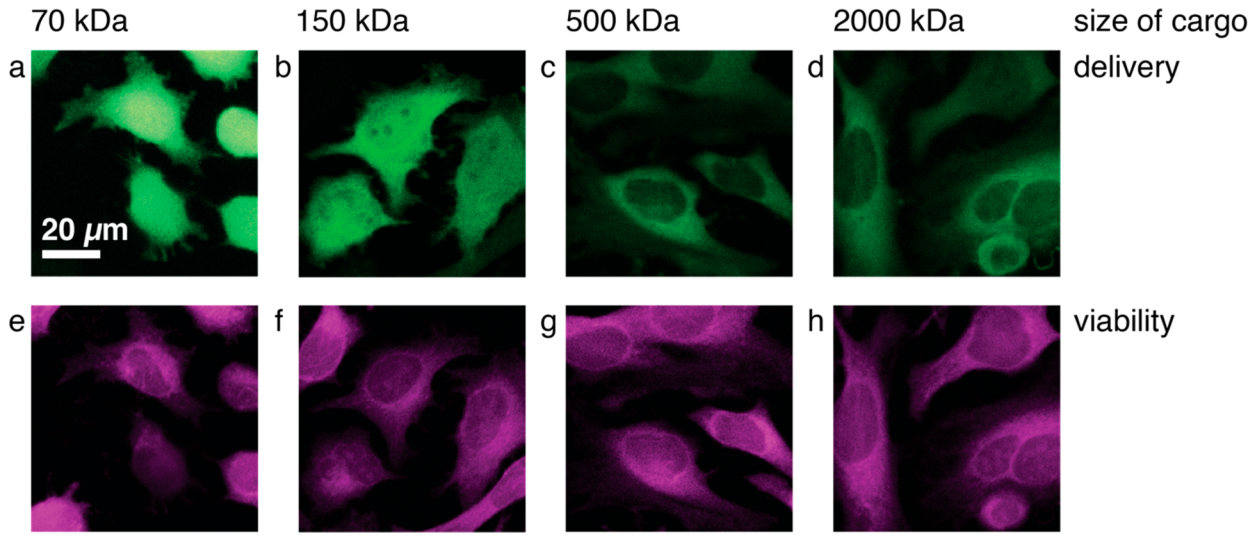

Figure 4. Intracellular delivery of large cargoes using self-assembled thermoplasmonic nanocavity substrates. (a–d) Confocal images of HeLa CCL-2 cells show green fluorescence, indicating delivery of FITC-dextrans (fluorescein isothiocyonate) ranging in size from 70 to 2000 kDa. Cargoes of 150 kDa and smaller are delivered to both the cytoplasm and the nucleus, whereas cargos 500 kDa and above are delivered to only the cytoplasm. (e–h) The same cells fluoresce after incubation with viability indicator calcein AM, indicating that all cells that are porated and that enclose the target molecules also exhibit healthy metabolic activity and remain viable.

possibility of delivering high molecular weight compounds via our thermoplasmonic nanocavity array, we performed proof-of-concept experiments aiming to deliver fluorescently labeled dextran macromolecules (fluorescein isothiocyanate (FITC) dextrans), with molecular weights ranging from 70 to 2000 kDa, to HeLa CCL-2 cells. We used the optimal fluence of 12.6 mJ cm^{-2}, as determined by the calcein green delivery experiments. The same laser scanning system and laser scanning parameters used in the calcein green delivery experiments were used in the FITC-dextran delivery experiments.

Figure 4a–d shows confocal fluorescence microscopy images of the cellular uptake of the different FITC-dextran polymers with molecular weights of 70, 150, 500, and 2000 kDaA. A fluorescence signal in the cell can be seen for all these molecular weights, indicating delivery of the cargo into to the cytoplasm of HeLa CCL-2 cells. Moreover, the 70 and 150 kDa FITC-dextrans appear to be delivered to the nuclei of the HeLa CCL-2 cells as well, as evidenced by the green fluorescence signal present throughout the entire region of the cell, including the nuclear region, in the confocal image slices. The intensity of the green fluorescence signal decreases for larger dextrans, indicating that the number of delivered molecules per cell decreases as the size of the delivered molecules increases. This is likely because the larger molecules diffuse more slowly, and therefore fewer molecules are able to diffuse into the cells before the pores in the cell membrane reseal. This inverse relation between delivery cargo size and the number of delivered molecules per cell is in agreement with results from other thermoplasmonic-substrate-based intracellular delivery techniques.[12] All cells that are successfully porated and encapsulated FITC-dextran also express a calcein AM signal, indicating they are viable after the experiment (Figure 4e–h). These proof-of-concept studies demonstrate the potential of the self-assembled thermoplasmonic nanocavity substrates to deliver large membrane-impermeable cargo to HeLa CCL-2 cells while maintaining cell viability. The ability to deliver large cargoes is crucial for applications such as footprint-free gene editing and imaging of intracellular organelles. Although the development of laser-activated thermoplasmonic substrates recently enabled high-throughput, high-efficiency, and high-viability intracellular delivery of large cargoes, the nanocavity substrates introduced here are the first to utilize a simple, quick, and cost-effective self-assembly-based fabrication process without necessitating the use of expensive and sophisticated cleanroom equipment.[10−13]

In conclusion, laser-activated self-assembled thermoplasmonic nanocavity substrates offer a promising intracellular delivery platform. We show spatially selective delivery of membrane-impermeable calcein green into HeLa CCL-2 cells, at a delivery efficiency of 78% and a cell viability of 87%. Additionally, we show successful delivery for diverse cargoes, ranging in size from 0.6 to 2000 kDa. The optimal laser fluence for the self-assembled nanocavity substrates is a factor of 5 smaller compared to similar thermoplasmonic substrates fabricated by nanofabrication. The spatially selective delivery enabled by these substrates opens the possibility of delivering cargoes to different cells or different regions of a tissue, which is important for generating complex tissues and studying interactions between subpopulations of cells.[29] In addition, the nanocavity substrates can be activated using a nanosecond-pulsed laser system, which is less expensive, easier to operate, and more stable than the femtosecond and picosecond laser systems that are required for many plasmonic materials for intracellular delivery.[8,13] The fabrication process is simple, quick, and cost-effective, making intracellular delivery experiments more accessible. The ability to efficiently deliver a range of membrane-impermeable cargoes into cells at high throughput while maintaining high cell viability, has the potential to advance the fields of biological and medical research by further enabling studies involving gene-editing, cellular engineering, imaging, and drug delivery.

DOI: 10.1021/acsabm.8b00447
ACS Appl. Bio Mater. 2018, 1, 1793−1799

■ ASSOCIATED CONTENT

Supporting Information

The Supporting Information is available free of charge on the ACS Publications website at DOI: 10.1021/acsabm.8b00447.

Description of the fabrication process for the self-assembled thermoplasmonic nanocavity substrates, simulations of laser energy absorption for metal-coated nanocavities, a description of the cell fixing protocol, a description of the fluorescence microscopy and cell counting methods, a description of the cell culture and seeding protocol, a description of the laser-scanning process and setup, and the results of a negative control experiment consisting of laser-activated delivery using unstructured glass coverslips coated with 50 nm of Ti (PDF)

■ AUTHOR INFORMATION

Corresponding Author

*E-mail: marinnamadrid@gmail.com.

ORCID

Marinna Madrid: 0000-0002-4305-8099
Nabiha Saklayen: 0000-0002-6336-080X
Nicolas Vogel: 0000-0002-9831-6905
Eric Mazur: 0000-0003-3194-9836

Author Contributions

⊥The manuscript was written through contributions of all authors. M.M. and N.S. contributed equally. All authors have given approval to the final version of the manuscript.

Notes

The authors declare the following competing financial interest(s): In accordance with ACS policy and our ethical obligations as researchers, Marinna Madrid and Nabiha Saklayen report an interest in Cellino Biotech, Inc., a company that may be affected by the research reported in the enclosed paper. Marinna Madrid and Nabiha Saklayen disclose those interests fully to ACS, and agree to manage any potential conflicts arising from said involvement. The other authors declare no conflict of interest.

■ ACKNOWLEDGMENTS

The research presented in this paper was supported by the National Science Foundation under Contract Nos. PHY-1219334 and PHY-1205465. M.M. was funded by the Graduate Prize Fellowship at Harvard Univ. N.S. was funded by the Howard Hughes Medical Institute's International Fellowship. N.V. acknowledges support by the Deutsche Forschungsgemeinschaft (DFG) under Grant No. VO 1824/5-1.

■ REFERENCES

(1) Rusk, N. Seamless Delivery. *Nat. Methods* **2011**, *8* (1), 44.

(2) Meacham, J. M.; Durvasula, K.; Degertekin, F. L.; Fedorov, A. G. Physical Methods for Intracellular Delivery: Practical Aspects from Laboratory Use to Industrial-Scale Processing. *J. Lab. Autom.* **2014**, *19* (1), 1−18.

(3) Antkowiak, M.; Torres-Mapa, M. L.; Stevenson, D. J.; Dholakia, K.; Gunn-Moore, F. J. Femtosecond Optical Transfection of Individual Mammalian Cells. *Nat. Protoc.* **2013**, *8* (6), 1216−1233.

(4) Baffou, G.; Berto, P.; Bermúdez Ureña, E.; Quidant, R.; Monneret, S.; Polleux, J.; Rigneault, H. Photoinduced Heating of Nanoparticle Arrays. *ACS Nano* **2013**, *7* (8), 6478−6488.

(5) Pustovalov, V. K.; Smetannikov, A. S.; Zharov, V. P. Photothermal and Accompanied Phenomena of Selective Nanophotothermolysis with Gold Nanoparticles and Laser Pulses. *Laser Phys. Lett.* **2008**, *5* (11), 775−792.

(6) Boulais, E.; Lachaine, R.; Hatef, A.; Meunier, M. Plasmonics for Pulsed-Laser Cell Nanosurgery: Fundamentals and Applications. *J. Photochem. Photobiol., C* **2013**, *17*, 26−49.

(7) Baffou, G.; Polleux, J.; Rigneault, H.; Monneret, S. Super-Heating and Micro-Bubble Generation around Plasmonic Nanoparticles under Cw Illumination. *J. Phys. Chem. C* **2014**, *118* (9), 4890−4898.

(8) Heinemann, D.; Schomaker, M.; Kalies, S.; Schieck, M.; Carlson, R.; Murua Escobar, H.; Ripken, T.; Meyer, H.; Heisterkamp, A. Gold Nanoparticle Mediated Laser Transfection for Efficient siRNA Mediated Gene Knock down. *PLoS One* **2013**, *8* (3), e58604.

(9) Alkilany, A. M.; Murphy, C. J. Toxicity and Cellular Uptake of Gold Nanoparticles: What We Have Learned so Far? *J. Nanopart. Res.* **2010**, *12* (7), 2313−2333.

(10) Messina, G. C.; Dipalo, M.; La Rocca, R.; Zilio, P.; Caprettini, V.; Proietti Zaccaria, R.; Toma, A.; Tantussi, F.; Berdondini, L.; De Angelis, F. Spatially, Temporally, and Quantitatively Controlled Delivery of Broad Range of Molecules into Selected Cells through Plasmonic Nanotubes. *Adv. Mater.* **2015**, *27*, 7145−7149.

(11) Courvoisier, S.; Saklayen, N.; Huber, M.; Chen, J.; Diebold, E. D.; Bonacina, L.; Wolf, J. P.; Mazur, E. Plasmonic Tipless Pyramid Arrays for Cell Poration. *Nano Lett.* **2015**, *15* (7), 4461−4466.

(12) Wu, Y. C.; Wu, T. H.; Clemens, D. L.; Lee, B. Y.; Wen, X.; Horwitz, M. A.; Teitell, M. A.; Chiou, P. Y. Massively Parallel Delivery of Large Cargo into Mammalian Cells with Light Pulses. *Nat. Methods* **2015**, *12* (5), 439−444.

(13) Saklayen, N.; Huber, M.; Madrid, M.; Nuzzo, V.; Vulis, D. I.; Shen, W.; Nelson, J.; McClelland, A. A.; Heisterkamp, A.; Mazur, E. Intracellular Delivery Using Nanosecond-Laser Excitation of Large-Area Plasmonic Substrates. *ACS Nano* **2017**, *11* (4), 3671−3680.

(14) Vogel, N.; Retsch, M.; Fustin, C. A.; Del Campo, A.; Jonas, U. Advances in Colloidal Assembly: The Design of Structure and Hierarchy in Two and Three Dimensions. *Chem. Rev.* **2015**, *115* (13), 6265−6311.

(15) Kraus, T.; Brodoceanu, D.; Pazos-Perez, N.; Fery, A. Colloidal Surface Assemblies: Nanotechnology Meets Bioinspiration. *Adv. Funct. Mater.* **2013**, *23* (36), 4529−4541.

(16) Stein, A.; Wilson, B. E.; Rudisill, S. G. Design and Functionality of Colloidal-Crystal-Templated Materials—Chemical Applications of Inverse Opals. *Chem. Soc. Rev.* **2013**, *42* (7), 2763−2803.

(17) Phillips, K. R.; England, G. T.; Sunny, S.; Shirman, E.; Shirman, T.; Vogel, N.; Aizenberg, J. A Colloidoscope of Colloid-Based Porous Materials and Their Uses. *Chem. Soc. Rev.* **2016**, *45* (2), 281−322.

(18) Vogel, N.; Weiss, C. K.; Landfester, K. From Soft to Hard: The Generation of Functional and Complex Colloidal Monolayers for Nanolithography. *Soft Matter* **2012**, *8* (15), 4044−4061.

(19) Nemiroski, A.; Gonidec, M.; Fox, J. M.; Jean-Remy, P.; Turnage, E.; Whitesides, G. M. Engineering Shadows to Fabricate Optical Metasurfaces. *ACS Nano* **2014**, *8* (11), 11061−11070.

(20) Ye, X.; Qi, L. Two-Dimensionally Patterned Nanostructures Based on Monolayer Colloidal Crystals: Controllable Fabrication, Assembly, and Applications. *Nano Today* **2011**, *6* (6), 608−631.

(21) Chen, X.; Chen, Y.; Yan, M.; Qiu, M. Nanosecond Photothermal Effects in Plasmonic Nanostructures. *ACS Nano* **2012**, *6* (3), 2550−2557.

(22) Baffou, G.; Quidant, R. Thermo-plasmonics: Using Metallic Nanostructures as Nano-sources of Heat. *Laser Photonics Rev.* **2013**, *7*, 171−187.

(23) Wang, Y.; Zaytsev, M. E.; The, H. L.; Eijkel, J. C. T.; Zandvliet, H. J. W.; Zhang, X.; Lohse, D. Vapor and Gas-Bubble Growth Dynamics around Laser-Irradiated, Water-Immersed Plasmonic Nanoparticles. *ACS Nano* **2017**, *11* (2), 2045−2051.

(24) Vogel, N.; Goerres, S.; Landfester, K.; Weiss, C. K. A Convenient Method to Produce Close- and Non-Close-Packed Monolayers Using Direct Assembly at the Air-Water Interface and

DOI: 10.1021/acsabm.8b00447
ACS Appl. Bio Mater. 2018, 1, 1793−1799

Subsequent Plasma-Induced Size Reduction. *Macromol. Chem. Phys.* **2011**, *212* (16), 1719−1734.
(25) Utech, S.; Bley, K.; Aizenberg, J.; Vogel, N. Tailoring Re-Entrant Geometry in Inverse Colloidal Monolayers to Control Surface Wettability. *J. Mater. Chem. A* **2016**, *4*, 1−7.
(26) Vogel, N.; Belisle, R. A.; Hatton, B.; Wong, T. S.; Aizenberg, J. Transparency and Damage Tolerance of Patternable Omniphobic Lubricated Surfaces Based on Inverse Colloidal Monolayers. *Nat. Commun.* **2013**, *4*, 2167.
(27) Yeung, H.; Neira, J.; Lane, B.; Fox, J. Laser Path Planning and Power Control Strategies for Powder Bed Fusion Systems. *Solid Freeform* **2016**, *27*, 113−127.
(28) O'Mahony, A. M.; Godinho, B. M. D. C.; Cryan, J. F.; O'Driscoll, C. M. Non-Viral Nanosystems for Gene and Small Interfering RNA Delivery to the Central Nervous System: Formulating the Solution. *J. Pharm. Sci.* **2013**, *102* (10), 3469−3484.
(29) Park, H. G.; Carmel, J. B. Selective Manipulation of Neural Circuits. *Neurotherapeutics* **2016**, *13* (2), 311−324.

DOI: 10.1021/acsabm.8b00447
ACS Appl. Bio Mater. 2018, 1, 1793−1799